Available online at www.sciencedirect.com
SCIENCE DIRECT®
Journal of Sound and Vibration 286 (2005) 817–847
JOURNAL OF SOUND AND VIBRATION
www.elsevier.com/locate/jsvi

Sound transmission through lightweight double-leaf partitions: theoretical modelling

J. Wang[a], T.J. Lu[b,*], J. Woodhouse[b], R.S. Langley[b], J. Evans[c]

[a]*School of Aeronautical Engineering, Queen's University, Belfast, UK*
[b]*Department of Engineering, University of Cambridge, Trumpington Street, Cambridge CB2 1PZ, UK*
[c]*Banro Holdings Ltd., Manor Works, Pleck Road, Walsall, West Midlands WS2 9ES, UK*

Received 2 October 2003; received in revised form 8 October 2004; accepted 19 October 2004
Available online 22 December 2004

Abstract

This paper presents theoretical modelling of the sound transmission loss through double-leaf lightweight partitions stiffened with periodically placed studs. First, by assuming that the effect of the studs can be replaced with elastic springs uniformly distributed between the sheathing panels, a simple smeared model is established. Second, periodic structure theory is used to develop a more accurate model taking account of the discrete placing of the studs. Both models treat incident sound waves in the horizontal plane only, for simplicity. The predictions of the two models are compared, to reveal the physical mechanisms determining sound transmission. The smeared model predicts relatively simple behaviour, in which the only conspicuous features are associated with coincidence effects with the two types of structural wave allowed by the partition model, and internal resonances of the air between the panels. In the periodic model, many more features are evident, associated with the structure of pass- and stop-bands for structural waves in the partition. The models are used to explain the effects of incidence angle and of the various system parameters. The predictions are compared with existing test data for steel plates with wooden stiffeners, and good agreement is obtained.

*Corresponding author. Tel.: +44 1223 766316; fax: +44 1223 332662.
E-mail address: tjl21@cam.ac.uk (T.J. Lu).

0022-460X/$ - see front matter © 2004 Elsevier Ltd. All rights reserved.
doi:10.1016/j.jsv.2004.10.020

Nomenclature

A_1, A_2	amplitudes of waves in cavity
c_0	sound speed in air
c_B	bending wave speed in panel
D_i	bending stiffness of panel
E_i	Young's modulus
f	frequency
h_i	panel thickness
H	separation distance between panels
I	incident wave amplitude
I_i	incident sound intensity
I_t	transmitted sound intensity
I_z	second moment of area about z-axis of stud
j	$\sqrt{-1}$
k_x, k_y	wavenumber in x- and y-direction
K_t	translational stiffness of stud
K'_t	uniformly distributed translational stiffness of stud
K'_r	uniformly distributed rotational stiffness of stud
K_r	rotational stiffness of stud
l	web length of stud
L	stud spacing
m_{pi}	panel's mass per unit area
M	half stud mass per unit length
M_b	bending moment
p	pressure perturbation
R	reflection wave amplitude
RL	transmission loss
s'	equivalent stiffness of air
t_0	wall thickness of stud
t	time
T	transmitted wave amplitude
$\underline{u}_i$	fluid velocity of the sound wave
W_i	panel deflections
$\hat{W}_i$	amplitude of panel deflections
$\alpha_{i,n}$	deflection amplitudes of panels
β_n	amplitudes of reflected waves in the incident half-space
ε_n	amplitudes of transmitted waves through the front panel
ζ_n	amplitudes of reflected waves from the rear panel
ξ_n	amplitudes of transmitted waves to the transmitted half-space incidence angle, normally from 0 to 78
θ_b	rotation angle
v_I	Poisson's ratio
ρ_0	air density
ρ_i	density of material
Φ_I	velocity potentials
$\tau(\theta)$	transmission coefficient at incidence angle θ
τ	averaged transmission coefficient for all possible incidence angles
ω	angular frequency
η_i	material loss factors

1. Introduction

Partition walls consisting of cold-formed steel frames clad with plasterboard are widely used in building construction. Compared with traditional masonry constructions, they are lighter, easier, and quicker to assemble, and leave a cleaner building site. However, they need greater skill to design and construct, because the overall design (including strength, stiffness, and buckling) is much more complex. It is also more difficult to predict sound transmission loss (STL).

The simplest acoustic partitioning that has been studied is a double-leaf wall without structural connections [1–5]. This type of structure, if it could be built, would provide high STL. However, vertical beams called "studs" are needed for practical partitions to support structural loads, and these decrease the STL and also complicate theoretical modelling. A typical lightweight partition without sound-absorbent infill material is depicted in Fig. 1. Sound can travel through the air-gap

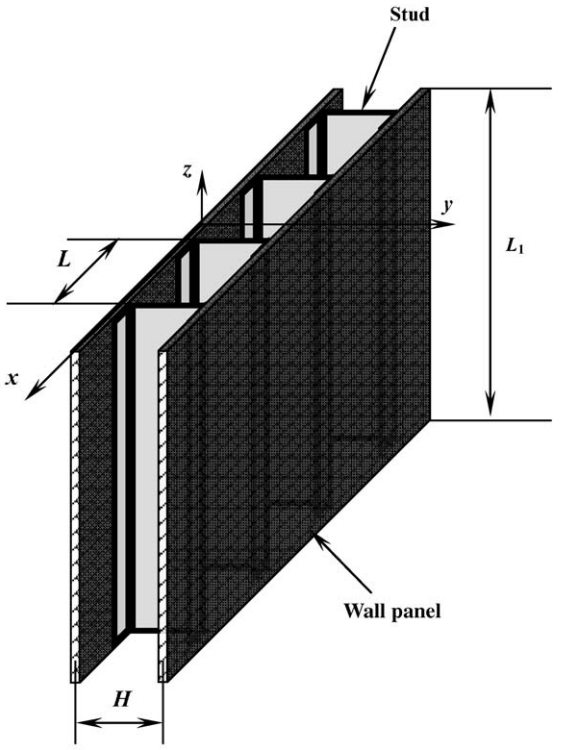

Fig. 1. Illustration of a double-leaf partition wall with studs.

between the two boards, and also the steel frame provides a structural route for sound transmission. The frame alters the dynamic and sound radiation properties of each panel, and thus changes the sound transmission of the partition wall as a whole [4]. Although a real structure will never be precisely periodic, periodic structure theory offers the most natural way to develop a theoretical model that takes account of the dominant features of the system [6–8]. Simple modelling of this kind will be presented in this paper. The aim of the research is to establish physically based models of sufficient accuracy that they can in due course be used in conjunction with optimisation techniques to design more efficient soundproofing partitions. The present paper represents only the first stage of this endeavour, since there are limitations to the models developed here which will be explained later.

Sharp [9] has discussed sound transmission through a double panel with sound bridges, by analysing the power radiated from a point- or line-loaded panel based on Cremer and Heckl's theory [10] using the impedance method, leading to an empirical method for predicting the STL. However, this method does not provide a sufficiently complete understanding of STL mechanisms to allow acoustic optimisation to be performed. Desmet and Sas [11] presented a method of finding sound transmission properties of a finite double-leaf partition at low frequencies, by experimental measurements as well as theoretical modelling based on Dowell's modal coupling theory [12]. Limited to low frequencies, this method is also not convenient for carrying out

optimisation studies. Lin and Garrelick [13], inspired by the work of Evseev [14], made use of Green's functions to solve the problem. In their work, the stud is assumed to be a rigid and massless coupling between the panels. Later, Urusovskii [15] pointed out that the basic equations of Lin and Garrelick [13] do not include the phase factor associated with the force exerted on the plates by the stud as a result of oblique incidence of a plane wave on the plates, nor is the mass reactance of the stud taken into account. The method adopted in Ref. [15] to describe the flexural deflection of the plates has some common aspects with the space-harmonic approach proposed by Mead [16] and Mead and Pujara [17]. However, the method still assumes that the studs join the plates rigidly, and does not take advantage of the periodicity of the system. In addition, no solution procedure or numerical results for the STL were presented. Takahashi [18] discussed sound radiation from periodically connected double-plate structures under mechanical excitation forces. Three different types of structure are considered: point connected, point connected with rib-stiffening, and rib-connected. However, acoustic loading as well as resonances in the cavity were ignored. Therefore, the results of Ref. [18] cannot be directly used to calculate sound transmission through double-leaf partitions.

Mead [16,19] studied the vibration response and wave propagation in periodic structures and discussed the characteristics of their propagation constants. Mead and Pujara [17] subsequently proposed to use space-harmonic expansions to study periodic partitions: they used a two-dimensional (2D) model in which the panel is represented as a beam supported b y regularly spaced elastic supports, which oppose both transverse displacement and rotation. This model is suitable for wave propagation perpendicular to the studs, i.e. in the horizontal plane for a partition wall. The response of the beam subjected to a homogeneous random convected pressure field was then solved. However, Mead and Pujara [17] pointed out that although the method has been devised for the estimation of sound radiation, acoustic effects were not actually included.

The space-harmonic method expresses the panel displacement and pressure field in terms of a series of travelling-wave harmonic terms. For a double-leaf partition, the system equations can be developed by combining the wave equation for sound waves in the incident, cavity and transmitted regions with the two beam equations, the latter including lumped masses and springs (translational and torsional) to represent the stud effects. By coupling the acoustic and structural vibrations with appropriate boundary conditions and then employing the virtual work principle, complete governing equations can be derived.

Mathur et al. [8] presented a theoretical model based on the space-harmonic approach to calculate STL through periodically stiffened panels and stiffened double-leaf structures: schemes to impose the structure-acoustic interactions and convergence criteria of the solution were developed. However, no solution procedure was given nor were any numerical results presented.

Lee and Kim [20] adopted the approach proposed by Mead and Pujara [17] and the schemes developed by Mathur et al. [8] to solve the vibro-acoustic equation of a single stiffened plate subjected to a plane wave input. An exact analysis procedure was developed to calculate the STL through an infinitely long elastic panel stiffened by periodic parallel beams. The present work extends this approach to double-leaf partitions stiffened with studs. For simplicity in this initial study, Mead's assumption of a 2D model is retained. A complete, predictive model would need to allow for general oblique incidence of sound waves, but this is deferred to future work.

The overall aim of this research is to develop deterministic analytical tools, focusing on the performance of key individual components and validated with experimental data, that can provide a better physical understanding of the STL mechanisms in double-leaf partitions. For simplicity, the system is considered to be of infinite extent in the direction of the frames, and a harmonic incident wave in the horizontal plane is considered so that 1D periodic structure theory can be applied. Two analytical models are developed, one based on replacing the studs with uniformly distributed elastic springs and the other with periodically placed discrete masses, and translational and rotational springs. For periodic modelling, the space-harmonic method is employed. Material damping is introduced by using a complex Young's modulus.

2. Smeared model

2.1. Derivation of smeared model

The smeared model for stud connections follows the approach used by Cremer and Heckl [10] to study impact sound insulation of floating floors; a similar but simpler model has been used by Kropp and Rebillard [5] to study the airborne sound insulation of double wall constructions. This earlier work is extended here to give a consistent model which will relate in a very direct way to the more elaborate periodic model to be developed in the next section. For double-leaf partitions, the smeared model assumes that the studs can be replaced by translational and rotational springs uniformly distributed between the two panels. The stud mass is also distributed over the panels. The model is directly relevant if the stud spacing is sufficiently small (smaller than half the wavelength). Furthermore, as becomes clear later, it can provide approximate "backbone" solutions for the full problem.

2.1.1. System equations

For a stud of depth l, wall thickness t_0, and Young's modulus E, the force per unit length due to a stretch of the stud in the y-direction (see Figs. 1 and 2) by a distance Δl is $Et_0\Delta l/l$. Consequently, each stud can be modelled as a spring of translational stiffness $K_t = Et_0/l$ per unit length. Similarly, the stud has a rotational stiffness K_r which is estimated in this study by considering the web bending of the stud:

$$M_b = EI_z\theta_b/l \equiv K_r\theta_b, \tag{1}$$

where $I_z = t_0^3/12$ is the second moment of area about the z-axis, M_b is the bending moment, and θ_b is the rotation angle.

Fig. 2 depicts the double wall partition with stud connections and the corresponding smeared model. For simplicity, it is assumed that the studs are periodically distributed between two infinitely large panels, and not connected to each other in the transverse direction.

As illustrated in Fig. 2a, in the smeared model the studs are replaced by translational and rotational springs of stiffness K_t' and K_r' per unit area, uniformly distributed between the two board panels. If the spacing between the studs is L, then $K_t' = K_t/L = Et_0/Ll$ and $K_r' = K_r/L = EI_z/Ll$. The panels are taken to be isotropic, with thickness (h_1, h_2), and mass per unit area (m_{p1}, m_{p2}), respectively (Fig. 2b). Under these assumptions, the governing equations of motion for the

two panels are given by [5,21]

$$D_1 \frac{\partial^4 W_1(x,t)}{\partial x^4} + \left(m_{p1} + \frac{M}{L}\right) \frac{\partial^2 W_1(x,t)}{\partial t^2} + K_t'(W_1(x,t) - W_2(x,t)) - K_r' \frac{\partial^2}{\partial x^2}(W_1(x,t) - W_2(x,t)) - \mathrm{j}\omega\rho_0(\Phi_1 - \Phi_2) = 0, \tag{2a}$$

$$D_2 \frac{\partial^4 W_2(x,t)}{\partial x^4} + \left(m_{p2} + \frac{M}{L}\right) \frac{\partial^2 W_2(x,t)}{\partial t^2} + K_t'(W_2(x,t) - W_1(x,t)) - K_r' \frac{\partial^2}{\partial x^2}(W_2(x,t) - W_1(x,t)) - \mathrm{j}\omega\rho_0(\Phi_2 - \Phi_3) = 0, \tag{2b}$$

where Φ_i describes the velocity potentials of the acoustic fields, as will be defined shortly, and D_i is the flexural stiffness of the panel:

$$D_i = \frac{E_i h_i^3 (1 + \mathrm{j}\eta_i)}{12(1 - \nu_i^2)}. \tag{2c}$$

Here, η_i is the loss factor of the panel material [20], and E_i, ν_i are the Young's modulus and Poisson's ratio of the panel material. The loss factor depends strongly upon the type of material of interest: typical values from the literature are 0.00073–0.00153 for steel, 0.1–0.3 for plasterboard, and 0.0045–0.115 for wood [22]. It is also likely to depend on frequency. Significant terms in Eqs. (2a) and (b) are the third and fourth terms representing structural coupling, and the fifth term representing air loading as well as airborne coupling.

The waves in the incident, cavity, and transmission regions can be expressed in terms of their respective velocity potentials:

$$\Phi_1 = \mathrm{e}^{-\mathrm{j}k_x x}(I\mathrm{e}^{-\mathrm{j}k_y y} + R\mathrm{e}^{\mathrm{j}k_y y})\mathrm{e}^{\mathrm{j}\omega t}, \tag{3a}$$

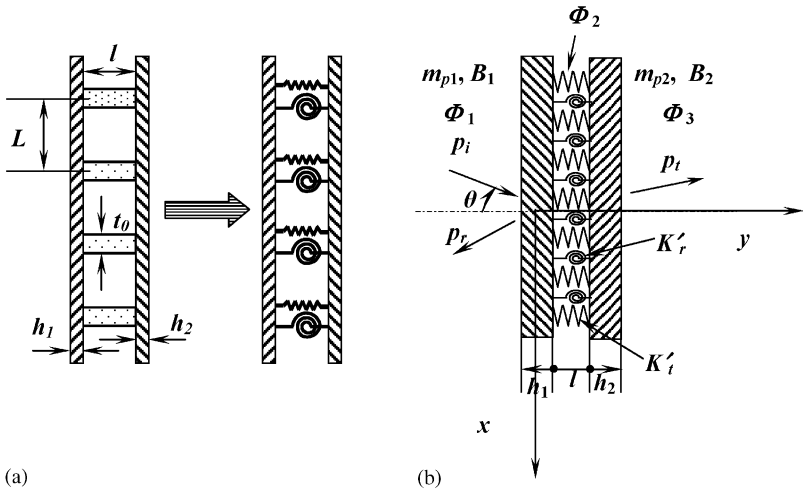

Fig. 2. Side view of a double-leaf partition wall with studs: (a) schematic of the smearing process and (b) notation used in the analysis.

$$\Phi_2 = \mathrm{e}^{-\mathrm{j}k_x x}(A_1\mathrm{e}^{-\mathrm{j}k_y y} + A_2\mathrm{e}^{\mathrm{j}k_y y})\mathrm{e}^{\mathrm{j}\omega t}, \tag{3b}$$

$$\Phi_3 = \mathrm{e}^{-\mathrm{j}k_x x}(T\mathrm{e}^{-\mathrm{j}k_y y})\mathrm{e}^{\mathrm{j}\omega t}, \tag{3c}$$

where ω is the angular frequency, I, R, and T are, respectively, the amplitude of the incident, reflected, and transmitted waves, and A_1, A_2 are the amplitudes of waves in the air cavity. The particle speed of the wave is related to the velocity potential by $\underline{u}_i = -\nabla\Phi_i$ $(i = 1, 2, 3)$. The corresponding pressure perturbation can be expressed as [4,7]

$$p = \rho_0 \frac{\partial \Phi}{\partial t} = \mathrm{j}\omega\rho_0\Phi \tag{4}$$

as used in Eqs. (2a) and (b). The wavenumber components k_x, k_y are given in terms of the angle of incidence θ via

$$k_x = k\,\sin\,\theta, \qquad k_y = k\,\cos\,\theta, \tag{5}$$

where $k = \omega/c_0$ and c_0 is the speed of sound in air.

Because the system is assumed to be infinite and homogeneous, the deflection of the two panels takes the following forms:

$$W_1(x, t) = \hat{W}_1\mathrm{e}^{-\mathrm{j}(k_x x - \omega t)}, \tag{6a}$$

$$W_2(x, t) = \hat{W}_2\mathrm{e}^{-\mathrm{j}(k_x x - \omega t)}. \tag{6b}$$

At the air–panel interface the normal velocity is continuous, resulting in the following coupling equations:

$$-\frac{\partial \Phi_1}{\partial y} = \mathrm{j}\omega W_1, \quad -\frac{\partial \Phi_2}{\partial y} = \mathrm{j}\omega W_1 \quad \text{at } y = 0, \tag{7a}$$

$$-\frac{\partial \Phi_2}{\partial y} = \mathrm{j}\omega W_2, \quad -\frac{\partial \Phi_3}{\partial y} = \mathrm{j}\omega W_2 \quad \text{at } y = H. \tag{7b}$$

2.1.2. Solution to the system equations

The sound transmission coefficient is defined by

$$\tau(\theta) = \left|\frac{T}{I}\right|^2. \tag{8}$$

The procedure to calculate $\tau(\theta)$ is as follows. Firstly, the boundary conditions, Eq. (7), are rewritten as

$$\begin{gathered}(\omega/k_y)\hat{W}_1 + R = I,\\ (\omega/k_y)\hat{W}_1 - A_1 + A_2 = 0,\\ (\omega/k_y)\hat{W}_2 - A_1\mathrm{e}^{-\mathrm{j}k_y H} + A_2\mathrm{e}^{\mathrm{j}k_y H} = 0,\\ (\omega/k_y)\hat{W}_2 - T\mathrm{e}^{-\mathrm{j}k_y H} = 0.\end{gathered} \tag{9}$$

Eq. (2) then become

$$[D_1k_x^4 - \omega^2 m_{p1} + K_t' + K_r'k_x^2 - M\omega^2/L]\hat{W}_1 - (K_t' + K_r'k_x^2)\hat{W}_2 - \mathrm{j}\omega\rho_0 R + \mathrm{j}\omega\rho_0(A_1 + A_2) = \mathrm{j}\omega\rho_0 I$$

and

$$-(K_t' + K_r'k_x^2)\hat{W}_1 + [D_2k_x^4 - \omega^2 m_{p2} + K_t' + K_r'k_x^2 - M\omega^2/L]\hat{W}_2 - \mathrm{j}\omega\rho_0(A_1\mathrm{e}^{-\mathrm{j}k_yH} + A_2\mathrm{e}^{\mathrm{j}k_yH}) + \mathrm{j}\omega\rho_0 T\mathrm{e}^{-\mathrm{j}k_yH} = 0.$$

By introducing

$$a_{11} = D_1k_x^4 - \omega^2 m_{p1} + K_t' + K_r'k_x^2 - M\omega^2/L - \frac{2\mathrm{j}\omega^2\rho_0\mathrm{e}^{\mathrm{j}k_yH}}{k_y(\mathrm{e}^{-\mathrm{j}k_yH} - \mathrm{e}^{\mathrm{j}k_yH})}, \tag{10a}$$

$$a_{12} = \frac{2\mathrm{j}\omega^2\rho_0}{k_y(\mathrm{e}^{-\mathrm{j}k_yH} - \mathrm{e}^{\mathrm{j}k_yH})} - K_t' - K_r'k_x^2 = a_{21}, \tag{10b}$$

$$a_{22} = D_2k_x^4 - \omega^2 m_{p2} + K_t' + K_r'k_x^2 - M\omega^2/L - \frac{2\mathrm{j}\omega^2\rho_0\mathrm{e}^{\mathrm{j}k_yH}}{k_y(\mathrm{e}^{-\mathrm{j}k_yH} - \mathrm{e}^{\mathrm{j}k_yH})}, \tag{10c}$$

the governing equations for panel motion can be expressed in matrix form as

$$\begin{bmatrix} a_{11} & a_{12} \\ a_{21} & a_{22} \end{bmatrix} \begin{Bmatrix} \hat{W}_1 \\ \hat{W}_2 \end{Bmatrix} = \begin{Bmatrix} 2\mathrm{j}\omega\rho_0 I \\ 0 \end{Bmatrix}. \tag{11}$$

Finally, from Eq. (11),

$$\hat{W}_2 = \frac{-2a_{12}\mathrm{j}\omega\rho_0 I}{a_{11}a_{22} - a_{12}a_{21}}$$

and

$$T = (\omega/k_y)\hat{W}_2\mathrm{e}^{\mathrm{j}k_yH} = \frac{-2a_{12}\mathrm{j}\omega^2\rho_0 I\mathrm{e}^{\mathrm{j}k_yH}}{k_y(a_{11}a_{22} - a_{12}a_{21})}$$

and hence

$$\tau(\theta) = \left|\frac{-2a_{12}\mathrm{j}\omega^2\rho_0\mathrm{e}^{\mathrm{j}k_yH}}{k_y(a_{11}a_{22} - a_{12}a_{21})}\right|^2. \tag{12}$$

The diffuse field transmission coefficient averaged over all angles of incidence within the incident plane is [4]

$$\tau = \frac{\int_0^{\pi/2} \tau(\theta)\sin\theta\cos\theta\,\mathrm{d}\theta}{\int_0^{\pi/2} \sin\theta\cos\theta\,\mathrm{d}\theta}. \tag{13}$$

Once τ is found, the transmission loss may be calculated:

$$RL = -10\log_{10}\tau. \tag{14}$$

2.2. Results of smeared model

Fig. 3 shows an example of the predicted STL using the smeared model for a plane wave at 45° incidence angle. The partition system consists of two identical 12.5 mm thick gypsum boards (Young's modulus $E = 7 \times 10^9\,\mathrm{N/m^2}$, Poisson's ratio $\nu = 0.3$, density $\rho = 1200\,\mathrm{kg/m^3}$) and periodically distributed C-section steel studs (Young's modulus $E_{\mathrm{stud}} = 210 \times 10^9\,\mathrm{N/m^2}$, wall thickness $t_0 = 0.5\,\mathrm{mm}$). The distance between the two panels is $H = 50\,\mathrm{mm}$ and the stud spacing is $L = 600\,\mathrm{mm}$. The translational stiffness of this particular design of the steel stud is given by

$$K_t = Et_0/l = 2.1 \times 10^9\,\mathrm{N/m}. \tag{15}$$

The rotational stiffness of the stud is estimated as

$$K_r = EI_z/l = 39.1\,\mathrm{Nm/rad}. \tag{16}$$

For uniformly distributed studs, the corresponding stiffnesses K'_t and K'_r are

$$K'_t = (Et_0)/(lL) = 3.125 \times 10^9\,\mathrm{N/m^3}, \tag{17a}$$

$$K'_r = (EI_z)/(lL) = 65.2\,\mathrm{N/rad}. \tag{17b}$$

The distributed mass of the studs is

$$M' = 2M/L = 0.884\,\mathrm{kg/m^2}. \tag{17c}$$

For this particular design the rotational stiffness and the stud mass have only a rather minor influence, but they are included for completeness.

Fig. 3 shows three curves of STL against frequency for this partition: the prediction of the complete smeared model, the prediction of the model with the stud properties (17) set to zero so that only airborne sound transmission is possible, and, for comparison, the "mass-law" curve [4]. As anticipated, both smeared model predictions follow the mass law at low frequencies, until a resonant phenomenon of one kind or another occurs which changes the sound transmission. Within the frequency range plotted, four frequencies of "resonance" occur, labelled f_1, f_2, f_3, and f_4. All four will be functions of the angle of incidence of the sound wave driving the partition.

The frequency f_1 is apparent only in the curve with airborne transmission alone. This is the so-called "mass-air-mass" resonance, at which the two panels move in opposite phase, bouncing on the "spring" of the air in the gap with equivalent stiffness $s' = (\rho_0 c_0^2)/H$. If the sound wave exciting the partition had been at normal incidence, this resonance would therefore have occurred at the frequency

$$f_1(0) = \frac{1}{2\pi}\sqrt{\frac{s'(m_{p1} + m_{p2})}{m_{p1}m_{p2}}}. \tag{18}$$

With the assumed angle of incidence of 45° the frequency is raised somewhat, as will be illustrated shortly.

The frequency f_2 occurs in both smeared model curves. This is the "coincidence frequency" for the panels, the frequency at which the wavelength of bending waves in the panels matches the trace wavelength of the incident wave [23]. The lowest value of this frequency occurs for a sound

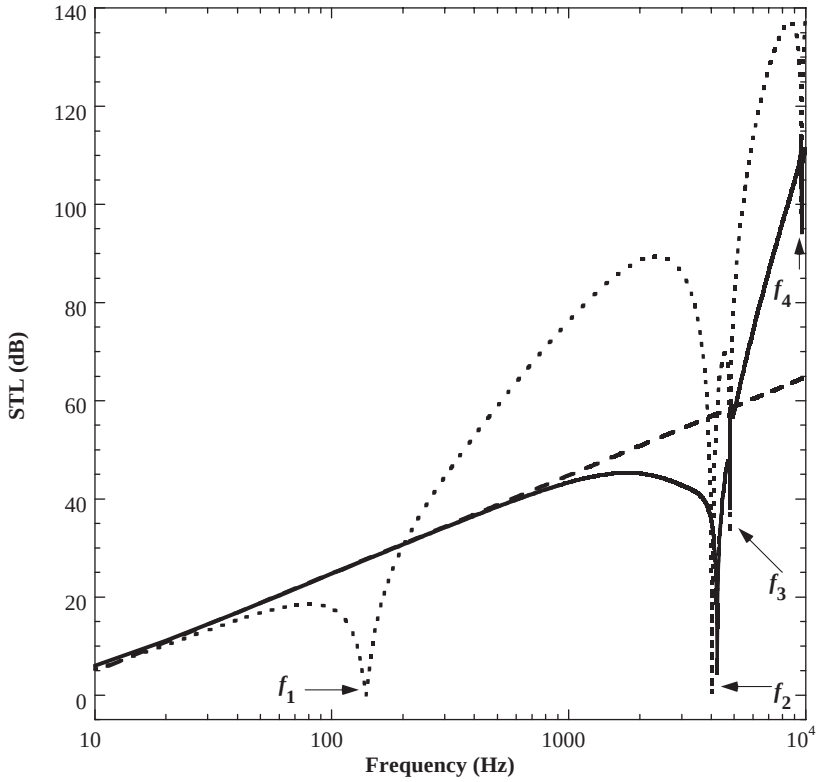

Fig. 3. STL for the smeared model for a wave incident at $\theta = 45^\circ$. The system properties are given in Table 1. Solid line: full smeared model; dotted line: smeared model without structural coupling; dashed line: mass-law transmission.

wave at grazing incidence, in which case the value would be

$$f_2(\pi/2) = \frac{c_0^2}{2\pi}\left\{\frac{12\rho(1-\nu^2)}{Et^2}\right\}^{1/2}. \tag{19}$$

The frequency is a little higher than this in Fig. 3, because of the assumed incidence angle.

Finally, the two frequencies f_3,f_4 correspond to a different physical phenomenon again: they are acoustic standing-wave resonances in the air-gap between the panels. There is a sequence of such resonances, having successive integer numbers of half-wavelengths in the width of the gap. The lowest resonance will have one half-wavelength, and will occur (for normal incidence of the sound wave) at

$$f_3(0) = c_0/(2H). \tag{20}$$

Again, the resonance appears at a slightly higher frequency in the plots because of the assumed angle of incidence.

Fig. 4 shows the result of varying the incidence angle in the full smeared model, plotted both as a surface and a contour map. The solid curve of Fig. 3 corresponds to the section through the surface of Fig. 4a at the incidence angle 45°. It is clear from this figure that there are four curves

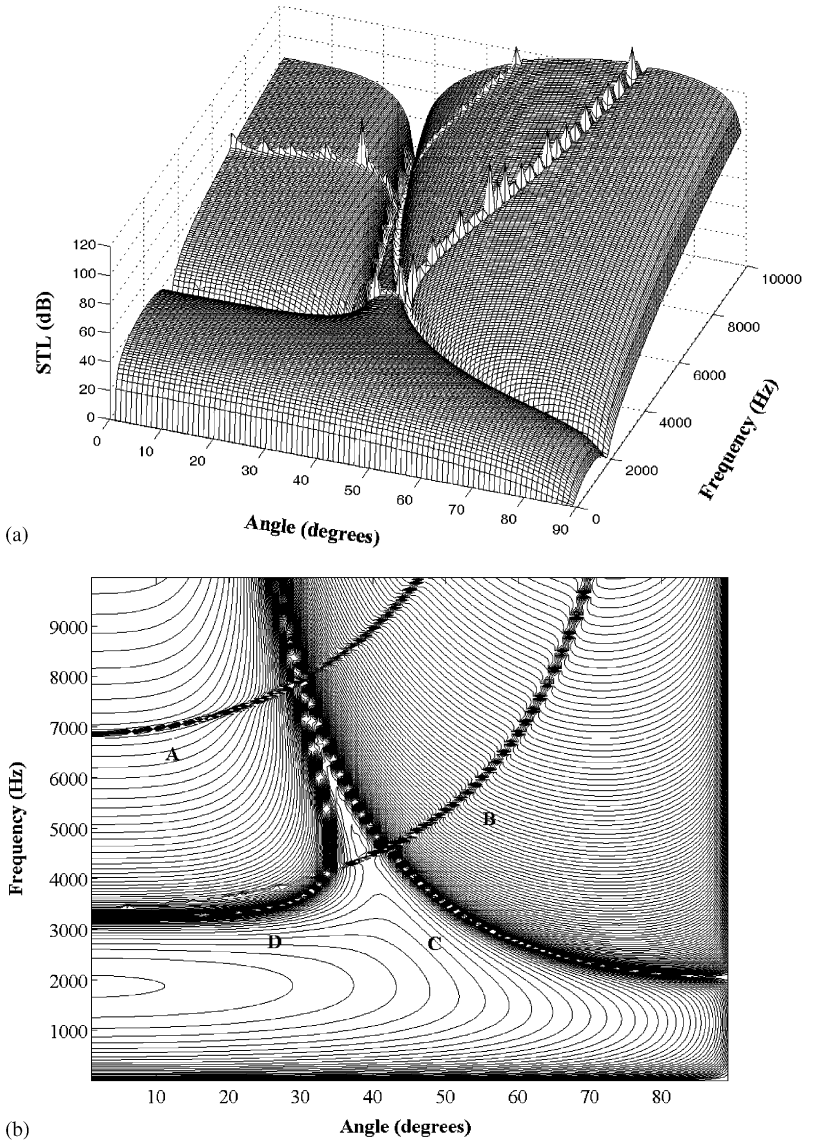

Fig. 4. (a) The variation of the STL with incidence angle and frequency for the smeared model. (b) Contour map of Fig. 4a.

that correspond to low STL, labelled A, B, C, and D in Fig. 4b. Curves A and B correspond to the acoustic resonances f_3,f_4. Curve C corresponds to the coincidence frequency f_2.

Curve D does not reach the angle 45°, so it was not seen in Fig. 3. To understand the origin of this curve it is convenient to examine the dispersion curves for bending waves travelling in the partition. Since the two panels can move independently, coupled through the distributed springs, there are two types of possible travelling waves. Since for this example the partition is symmetric

with respect to its centre plane, these two wave types consist of motion which is symmetric with respect to this plane, and motion which is antisymmetric. Antisymmetric motion simply implies that the two panels move in synchrony, with no relative motion across the springs. The dispersion characteristic is thus the same as for a single panel, as is plotted as the dash-dot curve in Fig. 5.

Symmetric motion involves "breathing" displacements of the two panels. Waves of this kind cannot propagate below a cut-on frequency at the equivalent of the "mass-air-mass" frequency, which will be significantly higher than the expression (18) because of the stiffening effect of the springs. Above this cut-on, the dispersion curve will show an approximately parabolic form similar to the curve for antisymmetric motion, and at very high frequencies, as panel bending comes to dominate the effect of the springs, the two curves tend to the same shape. The result is plotted as the solid line in Fig. 5.

Now consider an incident wave at a particular angle. The associated trace wavenumber will appear as a straight line in this plot as frequency is varied: an example for an incidence angle of 30° is shown as the dashed line in the figure. Wherever this straight line intersects one of the panel dispersion curves, a "coincidence" effect occurs. The intersection with the dash-dot curve is the normal coincidence frequency, already discussed. Intersections with the solid curve will correspond to coincidence with the symmetric waves in the partition, and this is the condition which generates the curve D in Fig. 4b. The shape of this curve can now be understood with reference to Fig. 5. As the angle of incidence is varied, the slope of the straight line varies from zero (at normal incidence) to a slope equal to the inverse of the speed of sound, shown as the dotted line in the figure. When the slope is low it intersects the dispersion curve twice and produces two "coincidence frequencies", whereas for steeper slopes there are no intersections. The re-entrant shape of curve D is thus explained.

3. Periodic model

3.1. Derivation of periodic model

Fig. 6 illustrates the periodic model of the partition. Each stud is modelled by translational and rotational springs together with lumped masses. A plane wave is incident on the left panel in area 1, which induces reflected waves, panel vibration, and transmitted waves into the cavity (area 2). The motion of the left panel is transferred to the right panel through the mechanical springs. In addition, the transmitted waves in the cavity become the incident waves on the right panel, which induce reflected waves in the cavity, motion of the right panel, and the final transmitted wave (area 3) through the partition.

To represent the panel vibration we make use of the key result of periodic structure theory, the Bloch or Floquet theorem [6]. The free motion of such a system can be represented as the product of two functions: a spatially periodic function with a period L (the stud spacing), and a bay-to-bay multiplicative factor, linking the motion of corresponding points in adjacent bays. A convenient form for the present problem is to express the motion of each panel as a "space-harmonic

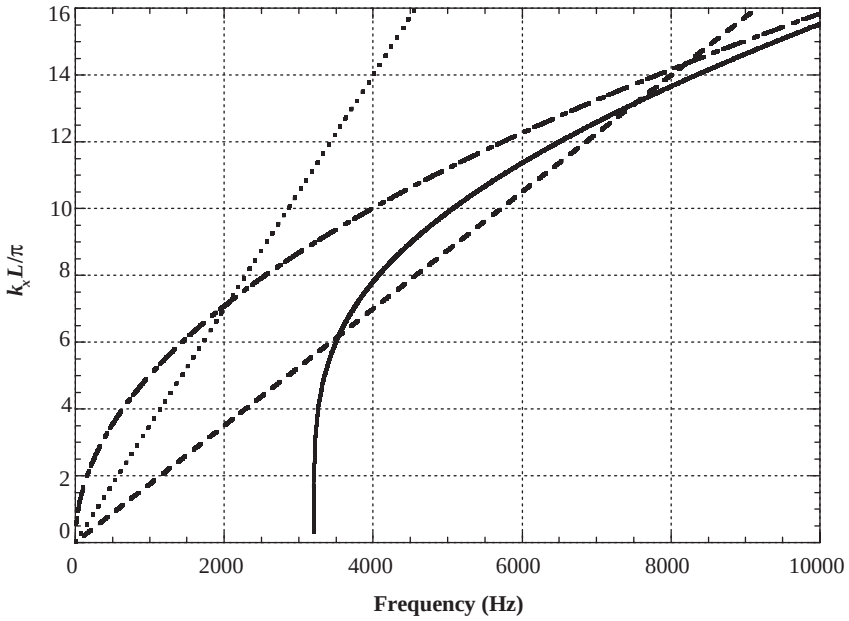

Fig. 5. Dispersion characteristics of the smeared model. Solid line: symmetric motion; dot-dashed line: antisymmetric motion; dashed line: acoustic wave at 30°; dotted line: acoustic wave at 90°.

expansion'', following Mead and Pujara [17]:

$$W_1(x,t) = \sum_{n=-\infty}^{+\infty} \alpha_{1,n} e^{-j[k_x+2n\pi/L]x} e^{j\omega t}, \tag{21a}$$

$$W_2(x,t) = \sum_{n=-\infty}^{+\infty} \alpha_{2,n} e^{-j[k_x+2n\pi/L]x} e^{j\omega t}, \tag{21b}$$

where $W_i(x,t)$ is the transverse displacement of the panel, coefficient $\alpha_{i,n}$ is the amplitude of the nth ''space harmonic'', and k_x is the component of the incident wavenumber in the x-direction, given by Eq. (5) as before. In Eq. (21), the terms with $[k_x + 2n\pi/L] > 0$ denote forward-travelling harmonic waves, while the terms with $[k_x + 2n\pi/L] < 0$ denote backward-travelling waves.

In a similar fashion, velocity potentials in the three different areas can be represented by space-harmonic series [17]. The velocity potential at an arbitrary point in the incident half-space is given by

$$\Phi_1(x,y,t) = I e^{-j[k_x x + k_y y - \omega t]} + \sum_{-\infty}^{+\infty} \beta_n e^{-j[(k_x+2n\pi/L)x - k_{yn} y - \omega t]}, \tag{22}$$

where the first and second terms represent the velocity potential of the incident and reflected waves, respectively. Similarly, the velocity potential in the cavity can be written as

$$\Phi_2(x,y,t) = \sum_{n=-\infty}^{+\infty} \varepsilon_n e^{-j\left[(k_x+2n\pi/L)x - k_{yn} y - \omega t\right]} + \sum_{n=-\infty}^{+\infty} \zeta_n e^{-j\left[(k_x+2n\pi/L)x - k_{yn} y - \omega t\right]}. \tag{23}$$

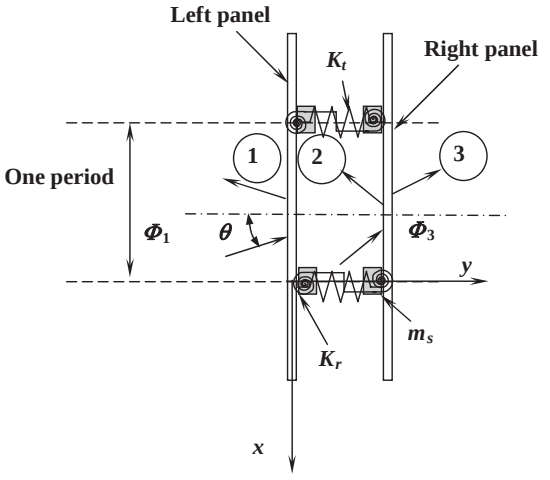

Fig. 6. A portion of the periodic double-leaf partition wall, and the notation used in the analysis.

In the transmitted area there is no reflected wave, so that

$$\Phi_3(x,y,t)=\sum_{n=-\infty}^{+\infty}\xi_n e^{-j[(k_x+2n\pi/L)x-k_{yn}y-\omega t]}. \tag{24}$$

Here, k_{yn} is the wavenumber in the y-direction, which can be calculated from [8,20]

$$k_{yn}=\sqrt{\left(\frac{\omega}{c}\right)^2-\left(k_x+\frac{2n\pi}{L}\right)^2}. \tag{25}$$

When $\omega/c<|k_x+2n\pi/L|$ the corresponding pressure waves become evanescent, and then the appropriate sign convention is to replace $jk_{yn}y$ in the exponent of Eq. (22) by $+\gamma_{yn}y$, where $\gamma_{yn}=\sqrt{(k_x+2n\pi/L)^2-(\omega/c)^2}$. Corresponding changes are made to Eqs. (23) and (24).

By substituting Eqs. (21)–(24) into the continuity conditions, Eq. (7) and cancelling the factor $e^{j\omega t}$ one arrives at

$$k_y I e^{-jk_x x}-\sum_{-\infty}^{+\infty}(k_{yn}\beta_n+\alpha_{1,n})e^{-j(k_x+2n\pi/L)x}=0, \tag{26a}$$

$$\sum_{n=-\infty}^{+\infty}[k_{yn}(\varepsilon_n-\zeta_n)-\omega\alpha_{1,n}]e^{-j(k_x+2n\pi/L)x}=0, \tag{26b}$$

$$\sum_{n=-\infty}^{+\infty}[k_{yn}(\varepsilon_n e^{-jk_{yn}H}-\zeta_n e^{jk_{yn}H})-\omega\alpha_{2,n}]e^{-j(k_x+2n\pi/L)x}=0, \tag{26c}$$

$$\sum_{n=-\infty}^{+\infty}[k_{yn}\xi_n e^{-jk_{yn}H}-\omega\alpha_{2,n}]e^{-j(k_x+2n\pi/L)x}=0. \tag{26d}$$

Because Eq. (26) should be valid at all values of x, the following relationships between the modal amplitudes are obtained:

$$\beta_0 = I - \omega\alpha_{1,0}/k_y, \tag{27a}$$

$$\beta_n = -\omega\alpha_{1,n}/k_{yn} \quad \text{at } n \neq 0, \tag{27b}$$

$$\varepsilon_n = \frac{\omega(\alpha_{2,n}e^{jk_{yn}H} - \alpha_{1,n}e^{2jk_{yn}H})}{k_{yn}(1 - e^{2jk_{yn}H})}, \tag{27c}$$

$$\zeta_n = \frac{\omega(\alpha_{2,n}e^{jk_{yn}H} - \alpha_{1,n})}{k_{yn}(1 - e^{2jk_{yn}H})}, \tag{27d}$$

$$\xi_n = \omega\alpha_{2,n}e^{jk_{yn}H}/k_{yn}. \tag{27e}$$

The coefficients $\alpha_{i,n}$ can be found by solving the system equations derived using the principle of virtual work for one bay of the partition [17,20]. The principle of virtual work states that the sum of the work done by all the elements in one bay of the system must equal zero when the system is subjected to any one of the virtual displacements [20]:

$$\delta W_i = \delta\alpha_{i,m}e^{-j(k_x+2n\pi/L)x}. \tag{28}$$

The total virtual work is the sum of the virtual work of the two panel elements, the virtual work by the translational and rotational springs, and a contribution from the lumped mass of studs.

3.1.1. Virtual work of panel elements

The equations governing the motion of the two panels are

$$D_1\frac{\partial^4 W_1}{\partial x^4} + m_{p1}\frac{\partial^2 W_1}{\partial t^2} - j\omega\rho_0(\Phi_1 - \Phi_2) = 0, \tag{29a}$$

$$D_2\frac{\partial^4 W_2}{\partial x^4} + m_{p2}\frac{\partial^2 W_2}{\partial t^2} - j\omega\rho_0(\Phi_2 - \Phi_3) = 0, \tag{29b}$$

where m_{pi} is the panel mass per unit area. The virtual work contributed by the two panel elements can then be represented as

$$\delta\Pi_{p1} = \int_{x=0}^{L}\left(D_1\frac{\partial^4 W_1}{\partial x^4} + m_{p1}\frac{\partial^2 W_1}{\partial t^2} - j\omega\rho_0(\Phi_1 - \Phi_2)\right)\delta W_1^* \,dx \quad \text{at } y = 0, \tag{30a}$$

$$\delta\Pi_{p2} = \int_{x=0}^{L}\left(D_2\frac{\partial^4 W_2}{\partial x^4} + m_{p2}\frac{\partial^2 W_2}{\partial t^2} - j\omega\rho_0(\Phi_2 - \Phi_3)\right)\delta W_2^* \,dx \quad \text{at } y = H, \tag{30b}$$

where δW_i^* represents the complex conjugate of the virtual displacement in Eq. (28). With Eqs. (21)–(24), Eq. (30) can be rewritten in terms of the amplitudes $\alpha_{i,n}, \beta_n, \varepsilon_n, \zeta_n$.

3.1.2. Virtual work of translational springs

$$\delta\Pi_{t1} = K_t(W_1(0) - W_2(0))\delta\alpha_{1,m}^* = K_t\left[\sum_{n=-\infty}^{+\infty}\alpha_{1,n} - \sum_{n=-\infty}^{+\infty}\alpha_{2,n}\right]\delta\alpha_{1,m}^*, \tag{31a}$$

$$\delta\Pi_{t2} = K_t(W_2(0) - W_1(0))\delta\alpha_{2,m}^* = K_t\left[\sum_{n=-\infty}^{+\infty}\alpha_{2,n} - \sum_{n=-\infty}^{+\infty}\alpha_{1,n}\right]\delta\alpha_{2,m}^*. \tag{31b}$$

3.1.3. Virtual work of rotational springs

$$\begin{aligned}\delta\Pi_{r1} &= K_r(W_1'(0) - W_2'(0))\mathrm{j}\left(k_x + \frac{2m\pi}{L}\right)\delta\alpha_{1m}^* \\ &= K_r\left[\sum_{n=-\infty}^{+\infty}\alpha_{1,n}\left(k_x + \frac{2n\pi}{L}\right) - \sum_{n=-\infty}^{+\infty}\alpha_{2,n}\left(k_x + \frac{2n\pi}{L}\right)\right]\left(k_x + \frac{2m\pi}{L}\right)\delta\alpha_{1,m}^*,\end{aligned} \tag{32a}$$

$$\begin{aligned}\delta\Pi_{r2} &= K_r(W_2'(0) - W_1'(0))\mathrm{j}\left(k_x + \frac{2m\pi}{L}\right)\delta\alpha_{2m}^* \\ &= K_r\left[\sum_{n=-\infty}^{+\infty}\alpha_{2,n}\left(k_x + \frac{2n\pi}{L}\right) - \sum_{n=-\infty}^{+\infty}\alpha_{1,n}\left(k_x + \frac{2n\pi}{L}\right)\right]\left(k_x + \frac{2m\pi}{L}\right)\delta\alpha_{2,m}^*,\end{aligned} \tag{32b}$$

where $W_i'(0) = \partial W_i(0)/\partial x$.

3.1.4. Virtual work of lumped masses

$$\delta\Pi_{m1} = -\omega^2 M W_1(0)\delta\alpha_{1,m}^* = -\omega^2 M\left[\sum_{n=-\infty}^{+\infty}\alpha_{1,n}\right]\delta\alpha_{1,m}^*, \tag{33a}$$

$$\delta\Pi_{m2} = -\omega^2 M W_2(0)\delta\alpha_{2,m}^* = -\omega^2 M\left[\sum_{n=-\infty}^{+\infty}\alpha_{2,n}\right]\delta\alpha_{2,m}^*, \tag{33b}$$

where $2M$ is the total mass of the stud per unit length.

3.1.5. Combined equation

Finally, from the principle of virtual work,

$$\delta\Pi_{pi} + \delta\Pi_{ti} + \delta\Pi_{ri} + \delta\Pi_{Mi} = 0 \quad (i = 1, 2), \tag{34}$$

one obtains

$$\left[D_1\left(k_x+\frac{2m\pi}{L}\right)^4-m_{p1}\omega^2-\frac{2\mathrm{j}\omega^2\rho_0\mathrm{e}^{2\mathrm{j}k_{ym}H}}{k_{ym}(1-\mathrm{e}^{2\mathrm{j}k_{ym}H})}\right]\alpha_{1,m}$$
$$+\frac{K_t-\omega^2M}{L}\left(\sum_{n=-\infty}^{+\infty}\alpha_{1,n}\right)+\frac{K_r}{L}\left[\sum_{n=-\infty}^{+\infty}\alpha_{1,n}\left(k_x+\frac{2n\pi}{L}\right)\right]\left(k_x+\frac{2m\pi}{L}\right)$$
$$-\frac{K_t}{L}\left(\sum_{n=-\infty}^{+\infty}\alpha_{2,n}\right)-\frac{K_r}{L}\left[\sum_{n=-\infty}^{+\infty}\alpha_{2,n}\left(k_x+\frac{2n\pi}{L}\right)\right]\left(k_x+\frac{2m\pi}{L}\right)$$
$$+\frac{2\mathrm{j}\omega^2\rho_0\mathrm{e}^{\mathrm{j}k_{ym}H}}{k_{ym}(1-\mathrm{e}^{2\mathrm{j}k_{ym}H})}\alpha_{2,m}=\begin{cases}2\mathrm{j}\omega\rho_0 I, & m=0,\\ 0, & m\neq 0\end{cases}\tag{35}$$

and

$$\left[D_2\left(k_x+\frac{2m\pi}{L}\right)^4-m_{p2}\omega^2-\frac{2\mathrm{j}\omega^2\rho_0\mathrm{e}^{2\mathrm{j}k_{ym}H}}{k_{ym}(1-\mathrm{e}^{2\mathrm{j}k_{ym}H})}\right]\alpha_{2,m}+\frac{K_t-\omega^2M}{L}\left(\sum_{n=-\infty}^{+\infty}\alpha_{2,n}\right)$$
$$+\frac{K_r}{L}\left[\sum_{n=-\infty}^{+\infty}\alpha_{2,n}\left(k_x+\frac{2n\pi}{L}\right)\right]\left(k_x+\frac{2m\pi}{L}\right)-\frac{K_t}{L}\left(\sum_{n=-\infty}^{+\infty}\alpha_{1,n}\right)$$
$$-\frac{K_r}{L}\left[\sum_{n=-\infty}^{+\infty}\alpha_{1,n}\left(k_x+\frac{2n\pi}{L}\right)\right]\left(k_x+\frac{2m\pi}{L}\right)+\frac{2\mathrm{j}\omega^2\rho_0\mathrm{e}^{\mathrm{j}k_{ym}H}}{k_{ym}(1-\mathrm{e}^{2\mathrm{j}k_{ym}H})}\alpha_{1,m}=0,\tag{36}$$

where use has been made of the coupling relations between the modal amplitudes of waves in air and flexural motion in panels defined in Eq. (27).

Eqs. (35) and (36), although a little messy, give a coupled set of linear equations which determine the coefficients $\alpha_{i,m}$. Once these coefficients are known, the remaining unknown coefficients $\beta_n, \varepsilon_n, \zeta_n$, and ξ_n are found by using Eq. (27). The power transmission coefficient can then be calculated as in Section 2.1.2, using

$$\tau(\theta)=\frac{\sum_{n=-\infty}^{n=+\infty}|\xi_n|^2\mathrm{Re}(k_{yn})}{|I|^2k_y}.\tag{37}$$

This result is based on the fact that the group velocity of the nth acoustic component in the y-direction is $\partial\omega/\partial k_{yn}=(k_{yn}/k_y)c$.

3.2. Relation between the two models

The smeared model derived in Section 2.1 is based on the assumption that uniformly distributed translational springs can be used in place of the discrete studs to link the two panels. It will be demonstrated below that, when the reflection of flexural waves in the panels at the stud joints is ignored, the periodic model reduces to the smeared model.

Following the same procedure as in Section 3.1 for the periodic model but replacing each summation over space harmonics by the single term $n = 0$, we obtain equations identical to Eqs. (3) and (6). After applying the coupling (boundary) conditions, Eq. (7), the unknown amplitudes R, A_1, A_2, and T can be obtained as

$$R = I - \omega/k_y \hat{W}_1, \tag{38a}$$

$$A_1 = \frac{\omega(\hat{W}_2 - \hat{W}_1 e^{jk_y H})}{k_y(e^{-jk_y H} - e^{jk_y H})}, \tag{38b}$$

$$A_2 = \frac{\omega(\hat{W}_2 - \hat{W}_1 e^{-jk_y H})}{k_y(e^{-jk_y H} - e^{jk_y H})}, \tag{38c}$$

$$T = \omega \hat{W}_2 e^{jk_y H}/k_y. \tag{38d}$$

Again, the amplitudes $\hat{W}_i$ are obtained by employing the principle of virtual work. The virtual displacement is defined as

$$\delta W_i = \delta \hat{W}_i e^{-j(k_x x - \omega t)}. \tag{39}$$

The total virtual work is comprised of the following components:

Panels

$$\delta \Pi_{p1} = \int_{x=0}^{L} \left(D_1 \frac{\partial^4 W_1}{\partial x^4} + m_{p1} \frac{\partial^2 W_1}{\partial t^2} - j\omega\rho_0(\Phi_1 - \Phi_2) \right) \delta W_1^* \, dx$$
$$= L\{D_1 k_x^4 \hat{W}_1 - m_1 \omega^2 \hat{W}_1 - j\omega\rho_0[I + R - A_1 - A_2]\} \delta \hat{W}_1^*, \tag{40a}$$

$$\delta \Pi_{p2} = \int_{x=0}^{L} \left(D_2 \frac{\partial^4 W_2}{\partial x^4} + m_{p2} \frac{\partial^2 W_2}{\partial t^2} - j\omega\rho_0(\Phi_2 - \Phi_3) \right) \delta W_2^* \, dx$$
$$= L\{D_2 k_x^4 \hat{W}_2 - m_2 \omega^2 \hat{W}_2 - j\omega\rho_0[A_1 e^{-jk_y H} + A_2 e^{jk_y H} - T e^{-jk_y H}]\} \delta \hat{W}_2^*. \tag{40b}$$

Translational springs

$$\delta \Pi_{ti} = K_t(W_i(0) - W_n(0))\delta W_i^* = K_t[\hat{W}_i - \hat{W}_n]\delta \hat{W}_i^*,$$
$$i, n = 1, 2, \quad i \neq n. \tag{41}$$

Rotational springs

$$\delta \Pi_{ri} = K_r(W_i'(0) - W_n'(0))j(k_x)\, \delta W_i^* = K_r[\hat{W}_i - \hat{W}_n](k_x)^2\, \delta \hat{W}_i^*,$$
$$i, n = 1, 2, \quad i \neq n. \tag{42}$$

Lumped mass

$$\delta \Pi_{mi} = -\omega^2 M W_i(0)\, \delta W_i^* = -\omega^2 M \hat{W}_i\, \delta \hat{W}_i^*, \quad i = 1, 2. \tag{43}$$

Substitution of Eqs. (41)–(44) into the principle of virtual work

$$\delta \Pi_{pi} + \delta \Pi_{ti} + \delta \Pi_{ri} + \delta \Pi_{Mi} = 0, \quad i = 1, 2 \tag{44}$$

leads to the same equation as that given by Eq. (11).

The above manipulation demonstrates that, when the reflected flexural wave at each stud point is ignored, the periodic model is equivalent to the smeared model with air loading. Physically, when the studs are uniformly distributed across the whole panel area, the partition system becomes homogeneous and all the reflected flexural waves from the stud points disappear.

3.3. Convergence check

The first stage of numerical calculation using the periodic model is to establish how many terms are needed to ensure convergence of the solution. Fig. 7a shows the plots of STL versus frequency for various numbers of terms, for a particular partition structure whose parameters are listed in Table 1. About 30 terms are needed for the solution to converge. To further demonstrate the convergence, the following frequencies, $f = 200$, 1000, 5000, and 10,000 Hz are chosen and their convergence curves are shown in Figs. 7b. The number of terms needed in the calculation increases with the frequency. At low frequencies, a few terms are enough to ensure the convergence. At higher frequencies ($\sim$10,000 Hz), 33 terms are needed to ensure the resulting error ($\sim$0.008 dB) is less than the pre-set error band of 0.01 dB.

Following Lee and Kim [20], it is assumed that once the solution converges at a given frequency, it converges for all lower frequencies. This assumption is valid for the example shown in Fig. 7, where the number of terms, 33, determined at the highest frequency of interest, 10,000 Hz, ensures that the solution converges for all other lower frequencies. The following iteration strategy is thence employed. The STL is first calculated at the highest frequency of interest, with progressively more terms in the series expansion. The solution is deemed to have converged once the difference between the STLs calculated at two successive calculations falls within a pre-set error band: the corresponding number of terms is then used to calculate the STL at all other frequencies.

4. Results and discussion

The predictions from the smeared model are first compared with those from the periodic model, to explain the new physical phenomena introduced by the periodicity. To emphasise the main effects, material damping is ignored in both models. Next, effects of the incidence angle are presented for both models. Finally, to demonstrate the predictive capability of the periodic model, comparisons are made with recent experimental data on steel plates with wooden studs from Hongisto et al. [24].

4.1. Periodic model versus smeared model

Using the same partition system considered earlier, with parameter values as listed in Table 1, Fig. 8 shows the STL at 45° incidence angle predicted by the periodic model compared with that predicted by the smeared model. The periodic model follows the general trend of the smeared model, but it shows significant new features: peaks and dips in the STL relative to the smooth variation of the simpler model. The studs are necessary components of the partition in order to carry the structural loads, but it is clear that they behave like short circuits and cause

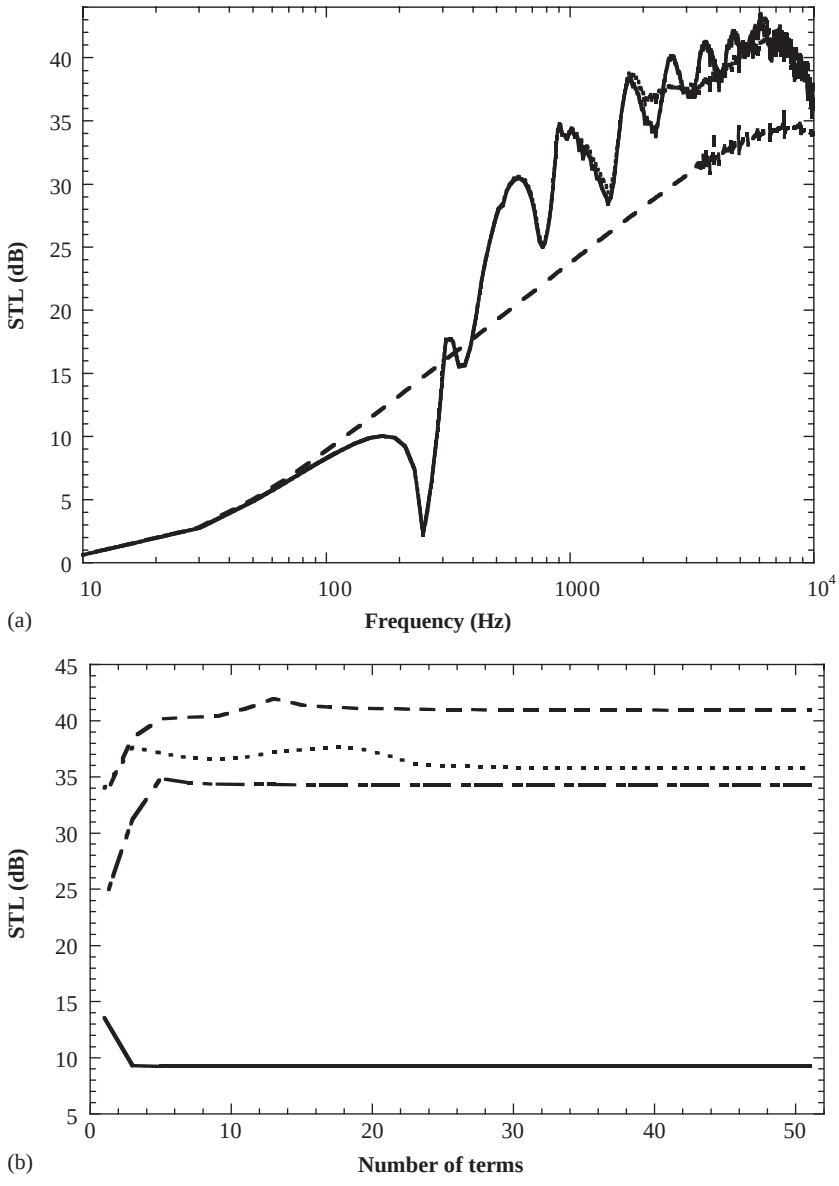

Fig. 7. Numerical convergence check for the system detailed in Table 1. (a) STL averaged over all possible incidence angles plotted against frequency. Solid line: 33 terms used; dash-dotted line: 15 terms; dotted line: seven terms; dashed line: one term. (b) STL averaged over all possible incidence angles plotted against number of terms used in the calculation. Solid line: 200 Hz; dot-dashed line: 1000 Hz; dashed line: 5000 Hz; dotted line: 10,000 Hz.

an increase of sound transmission in some frequency bands. The dips caused by the periodic properties of the structure are very significant for STL of partitions, and it is important to understand their physical origin.

Table 1
Panel dimensions and simulation data

K_t (N/m)	2.1×10^9	K_r (Nm/rad)	39.1	M (kg)	0.265
L (m)	0.600	E_1 (Pa)	7.0×10^9	E_2 (Pa)	7.0×10^9
ρ_0 (kg/m^3)	1.21	ρ_1 (kg/m^3)	1200	ρ_2 (kg/m^3)	1200
h_2 (m)	12.5×10^{-3}	h_1 (m)	12.5×10^{-3}	η_1	0.1
η_2	0.1	v_1	0.3	v_2	0.3
c_0 (m/s)	343				

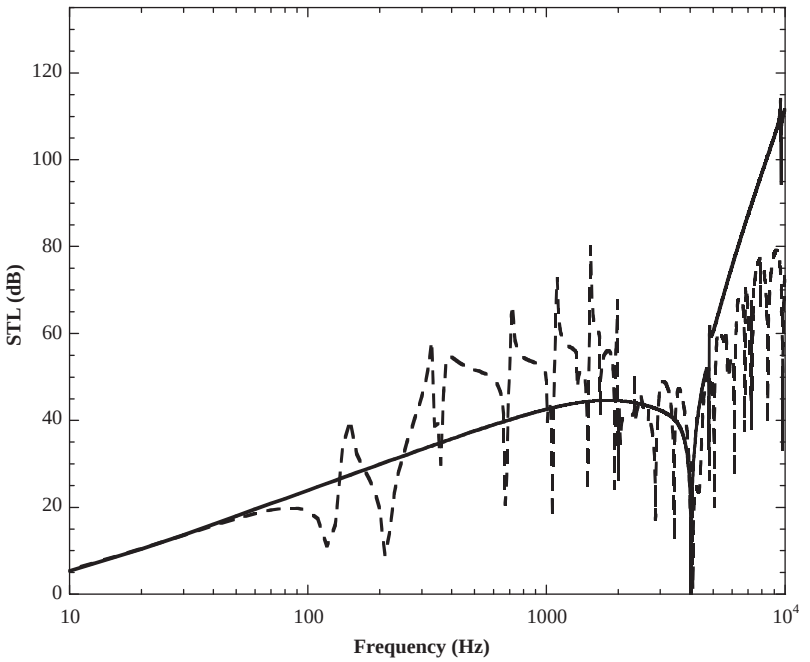

Fig. 8. Comparison of the STL yielded by the smeared and periodic models for the parameters listed in Table 1. Solid line: smeared model; dashed line: periodic model.

The dips in the STL curve correspond to frequencies where the incident sound wave undergoes a kind of resonance with the free-wave propagation of vibration in the panel. The effect is analogous to the familiar ''coincidence frequency'' discussed in Section 2.2, but the spatial harmonics created by wave reflection at the studs introduce multiple possibilities for wavenumber matching and ''coincidence''. To see what is happening it is necessary to examine briefly the structure-borne vibration response of the periodic system. For simplicity, the effects of air loading on the structural behaviour will be ignored for the moment. To include such effects makes the modelling more complicated without changing the qualitative picture.

Since the partition studied here has a symmetrical construction, the problem of structural vibration transmission in the partition can be decomposed into two parts, one in which the two panels move in a symmetrical way and one in which they move in an antisymmetrical way. The same argument was used earlier, in discussing Figs. 4 and 5. Symmetric motion (with respect to

the symmetry plane running through the centre of the partition) means that the panels move in "breathing" motion, both in or both out at a given position and a given time. For such motion, the stiffness of the studs imposes a strong constraint. Antisymmetric motion, on the other hand, involves the two panels moving in step. The studs are carried along by the panel motion, but since there is no relative motion at the two ends of a stud, the stud stiffness imposes no constraint. The mass of the studs has some influence on the motion, but this is small enough to be ignored for the present purpose.

The result is that the vibration propagation characteristics for antisymmetric motion are approximately the same as for a single panel with no studs, but for symmetric motion they are altered very significantly by the periodic studs. For the former case, a sinusoidal vibration can propagate along the partition at any frequency, with a wavenumber/frequency relation, or dispersion curve, which is parabolic as seen in Fig. 5. For the latter case, the most important effect of the periodicity is to divide the frequency range into a sequence of "pass bands", where vibration can propagate, and "stop bands", where it cannot (see, e.g., Refs. [6,7]). It is this pattern of stop and pass bands that is responsible for the peaks and dips in the STL shown in Fig. 8.

The rotational stiffness of these particular studs produces a negligible effect, so that by far the strongest effect, and the only one which need be kept here, is the translational stiffness of the studs. The resulting model of symmetrical vibration of the partition is very simple: relative to the centre plane of the partition, each panel vibrates as a beam restrained by periodically placed springs to "ground". This problem can be solved easily, for example by the transfer matrix method as used by Mead [16] for similar problems. The result of the calculation is shown in Fig. 9a, in which wavenumber is plotted against frequency. The pass bands for symmetrical motion appear as sinuous lines, because at a given frequency the travelling wave consists of a mixture of related wavenumbers having the same general form as Eq. (21). The dispersion curve for antisymmetric motion is also shown. The sloping dashed line indicates the behaviour of the incident sound wave at 45°. The shaded wedge indicates the region of the frequency/wavenumber plane in which waves in the partition can radiate sound. This wedge is bounded by the sound-speed lines corresponding to grazing incidence, parallel to the partition.

It is clear from Fig. 9a that within the frequency range plotted, the incident sound waves can never excite the antisymmetric motion strongly enough to be resonant—this does not occur until the coincidence frequency. For the symmetric motion, though, there are intersections of the dispersion curves, one per pass band. At each of these intersections the incident sound wave can excite panel vibration of sufficient amplitude that very strong sound transmission occurs, and this is the cause of the dips in the STL curve. This is demonstrated in Figs. 9b and c. Fig. 9b shows the "wrapped" version of Fig. 9a, obtained by "folding" the segments into the range $0-\pi$. This folding process gives a compact diagram which is often useful in periodic structure theory [7]. It is analogous to the effect of aliasing on the frequency spectrum of a sampled waveform: we are "sampling" the spatial structure once per bay. Fig. 9c, on the same frequency scale, shows the STL plot for this simplified problem with no stud mass or rotational stiffness, and no air coupling between the panels. It is immediately clear that the intersections labelled A, B, C, and D correspond to the positions of dips in Fig. 9c.

The intersections labelled A′, B′, C′, and D′ correspond to the peaks in the STL curve. The reason for this is much less obvious, since it is clear from Fig. 9a that these intersections are in some sense "not real", but an artefact of the wrapped plot. However, at these frequencies the

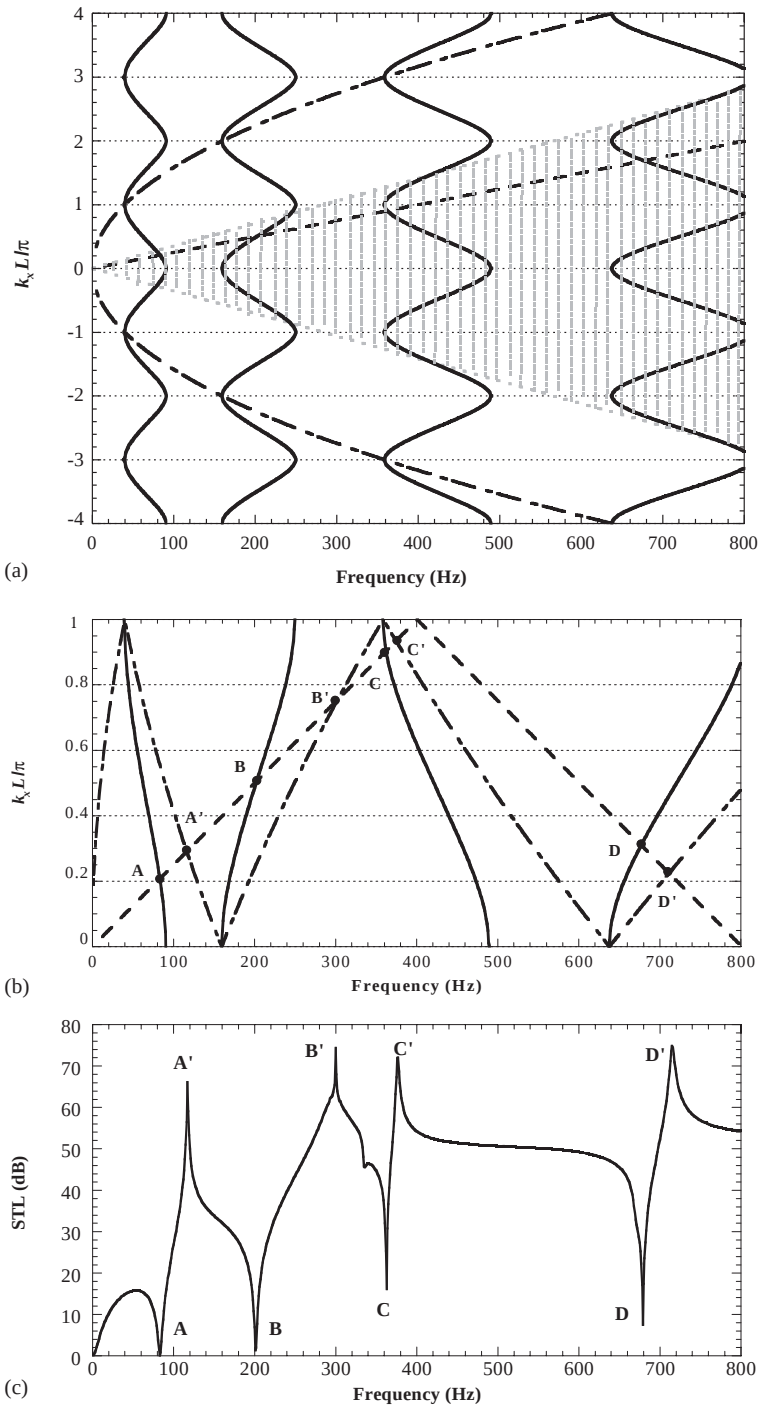

Fig. 9. (a) Normalised wavenumber $k_x L/\pi$ plotted against frequency. Solid line: the pass bands for symmetric motion; dot-dashed line: the dispersion curve for antisymmetric motion; dashed line: the dispersion curve for the incident sound at $\theta = 45^\circ$; shaded area: the region of the frequency/wavenumber plane for which bending waves in the partition can radiate sound. (b) The "wrapped" version of Fig. 9a. The normalised wavenumber $k_x L/\pi$ is plotted against frequency. Solid line: the pass bands for symmetric motion; dot-dashed line: the dispersion curve for antisymmetric motion; dashed line: the dispersion curve for the incident sound at $\theta = 45^\circ$. (c) STL plotted for the problem presented in Fig. 9a.

response of the panel exposed to the incident sound wave takes a particularly simple form in which only two terms of the sum in Eq. (21a) are needed: the directly driven term $n = 0$ and the term that satisfies the "coincidence" condition

$$D_1[k_x + 2N\pi/L]^4 = m_{p1}\omega^2. \tag{45}$$

The displacement of the driven panel is then

$$W_1 = I\mathrm{j}\omega\rho_0 \mathrm{e}^{\mathrm{j}\omega t}\mathrm{e}^{-\mathrm{j}k_x x}\left[\frac{1-\mathrm{e}^{-\mathrm{j}2N\pi x/L}}{D_1 k_x^4 - m_{p1}\omega^2}\right]. \tag{46}$$

This has nodal points at all the studs, so that no force is transmitted to the other panel, and therefore no sound is radiated.

The panel becomes a perfect reflector of sound at these frequencies. Fig. 10 shows the patterns of panel displacement (at $t = nT$, where $T = 2\pi/\omega$ is the period of vibration) corresponding to the first few frequencies of peaks and dips in Fig. 9c. It is not a surprise that this symmetrical partition model exhibits a sequence of frequencies of perfect reflection and perfect transmission: this is an example of a rather general result for wave transmission through symmetrical coupling systems [25].

When the coupling through the internal air is added back into the model the picture becomes somewhat more complicated, as shown in Fig. 11. The same qualitative features can be seen as in Fig. 9c: the main change is that there are extra dips in the STL curve, because the additional coupling through the air has made the structure of stop and pass bands more complicated. The physical explanation just given remains broadly correct.

Fig. 12 shows a series of STL calculations with the periodic model in which the stud spacing is varied while keeping the equivalent distributed stud stiffness K_t' fixed at $3.125 \times 10^9\,\mathrm{N/m^3}$. The rotational stiffness is set to zero because it has virtually no influence on the STL results for this particular design of stud. The curves are separated for clarity in the plot, and the result of the smeared model is included at the bottom. As the stud spacing decreases the system approaches, as expected, the case represented by uniformly distributed stud stiffness, i.e. the smeared model.

4.2. Effect of the incidence angle

For practical prediction of sound transmission performance, the results for a single angle of incidence are only of limited significance. What is needed is an appropriate average over all incidence angles. Ideally, this should be an average over all angles in a 3D sense, but the theory presented here only allows an average to be taken over angles in the plane normal to the studs. Fig. 13a shows the variation of STL with angle for the periodic mode for the same partition discussed above. This figure can be compared with Fig. 4a, for the smeared model. Fig. 13b shows the results of averaging over angle in both models.

It can be seen in Fig. 13a that the detailed features of the periodic model, discussed in the previous section, vary with incidence angle. The pattern can be understood with reference to Fig. 9b. The dips in the surface of Fig. 13a trace out portions of the pass bands, since the intersection points A, B, etc. move along the bands as the incidence angle is varied. Similarly, the

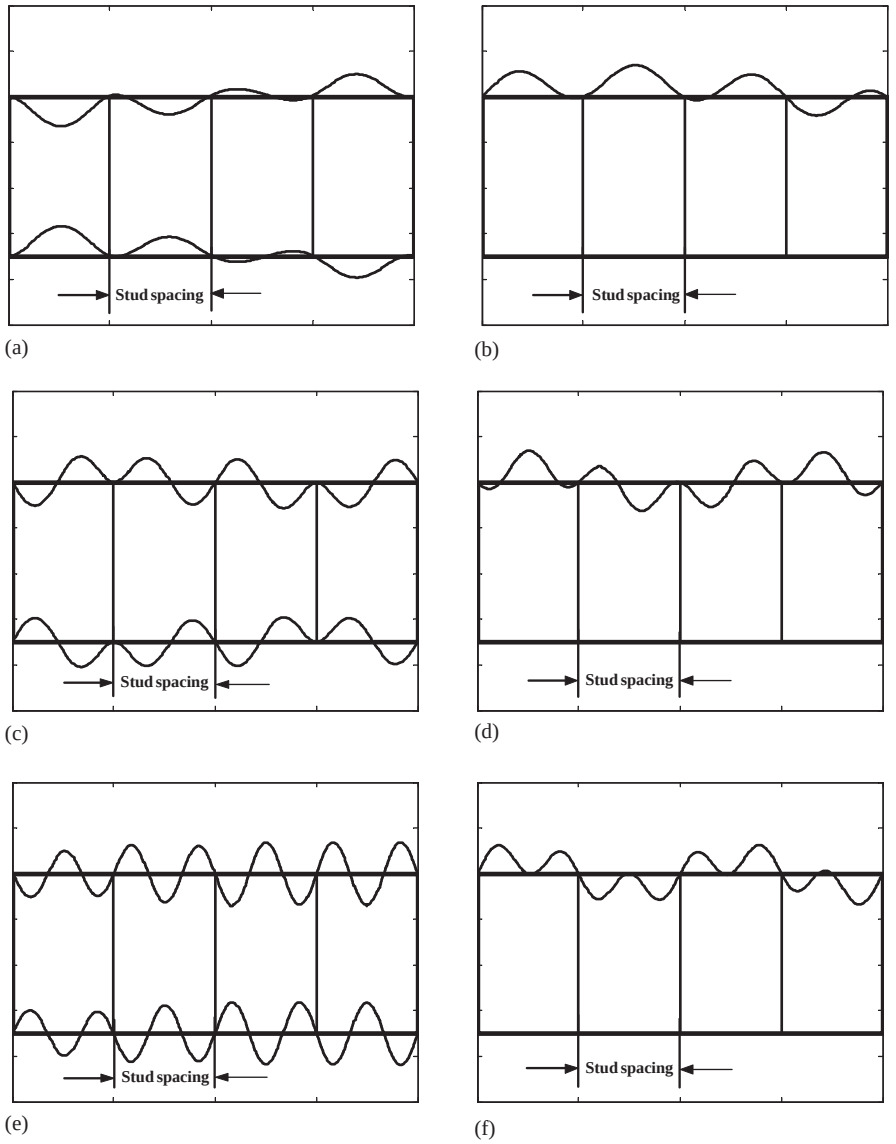

Fig. 10. The panel displacements corresponding to the first few peak and trough frequencies shown in Fig. 9c. The displacements are shown at a time corresponding to $t = nT$, where T is the period of the motion. (a) 83 Hz; (b) 117 Hz; (c) 203 Hz; (d) 301 Hz; (e) 363 Hz; (f) 376 Hz.

ridges in the surface trace out patterns recognisably related to the "wrapped" version of the panel dispersion curve, like the dot-dashed line in Fig. 9b. Much of this detail is lost when an average is taken over incidence angles, and the resulting curve in Fig. 13b follows the curve for the smeared model much more closely than did the curves for individual incidence angles, such as seen in Fig. 8.

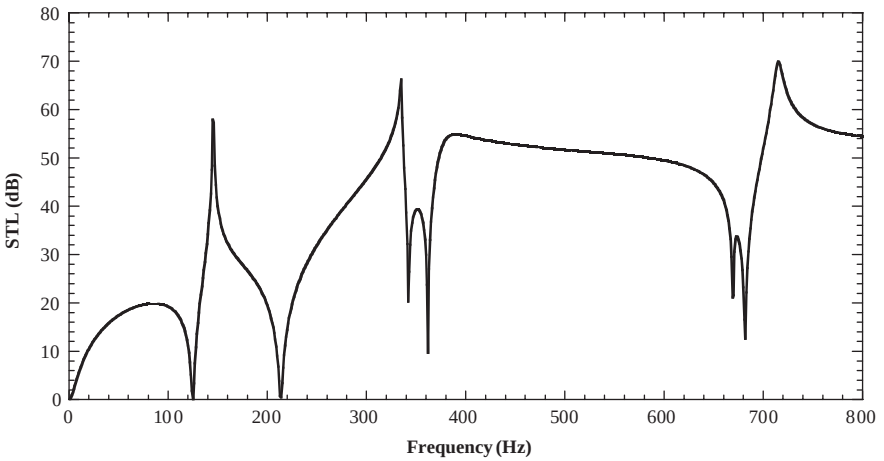

Fig. 11. STL plotted for the problem presented in Fig. 9a, with the addition of air in the cavity.

4.3. Comparison with measurements

Fig. 14 shows a comparison of the predictions from the periodic and smeared models developed here with test data taken from Fig. 12 of Hongisto et al. [24] for a double-leaf partition consisting of two identical 2 mm thick steel plates (Young's modulus $210 \times 10^9\,\mathrm{N/m^2}$ and density $7800\,\mathrm{kg/m^3}$) and wooden studs (thickness 120 nm and width 42 nm). The wooden studs are periodically distributed, with stud spacing of 1100 mm, and there is no sound absorbent present in the cavity. The air density is $\rho_0 = 1.25\,\mathrm{kg/m^3}$, and speed of sound is $c_0 = 343\,\mathrm{m/s}$. The simulation conditions are listed in Table 2. The predicted STL is obtained by averaging over all incidence angles.

From Fig. 14 it is seen that, although the STL curve predicted by the periodic theory is undulating due to the periodic nature of the model, it follows the correct trend of test data and, overall, the prediction agrees well with the data. Wooden studs are normally considered as rigid, since they have very high translational and rotational stiffness. The high stud stiffness causes strong wave reflections, which is the underlying reason for the "wavy" shape of the STL curve predicted by the periodic model. The smeared model yields a poor prediction of the STL for this case, as can be seen in Fig. 14. Better agreement of the present theories with experiment should probably not be expected because of the 2D nature of the models. In the measurement, the sound field was a fully diffuse 3D field.

5. Concluding remarks

Two analytic models have been developed to predict STL through double-leaf partition walls stiffened with studs. The smeared model assumes that the studs can be modelled using uniformly distributed springs and mass. In the periodic model, the studs are modelled as a set of periodically distributed lumped masses attached to the two panels, together with a set of periodically spaced

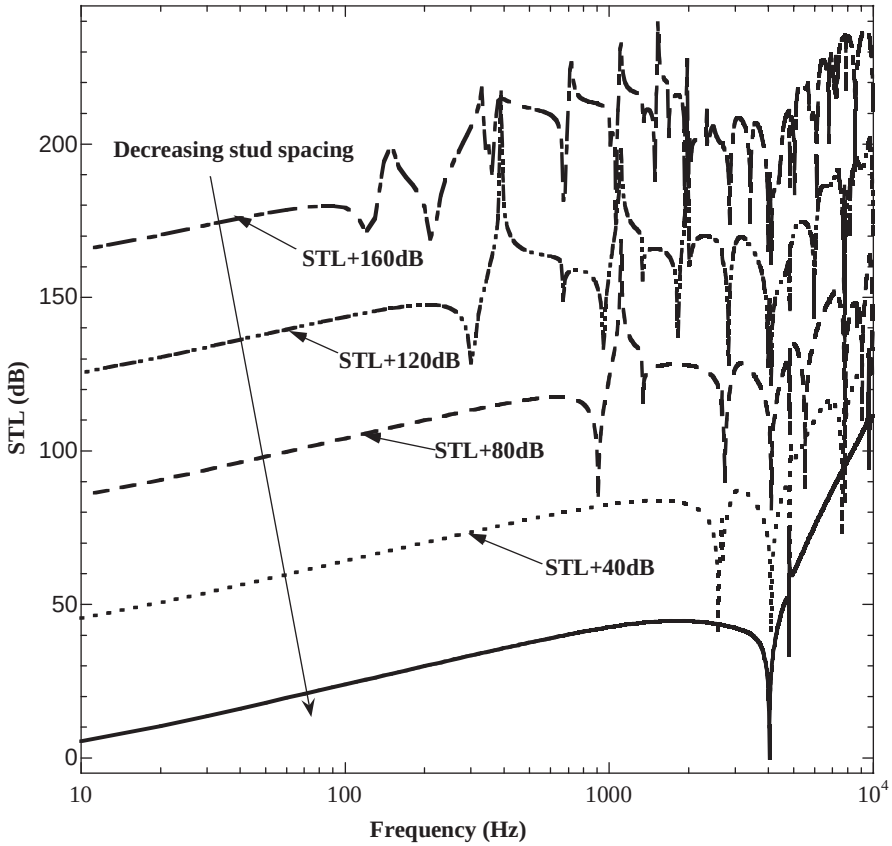

Fig. 12. STL for the periodic model for various stud spacings. Solid line: STL for smeared model ($K_t' = 3.125 \times 10^9\ \mathrm{N/m^3}$); dot-dashed line: STL for periodic model with stud spacing 600 mm ($K_t = 1.875 \times 10^9\ \mathrm{N/m^2}$); dot-dot-dashed line: stud spacing 300 mm ($K_t = 0.9375 \times 10^9\ \mathrm{N/m^2}$); dashed line: stud spacing 150 mm ($K_t = 0.46875 \times 10^9\ \mathrm{N/m^2}$); dotted line: stud spacing 75 mm ($K_t = 0.234375 \times 10^9\ \mathrm{N/m^2}$).

springs with rotational and translational stiffness. The dynamic equations that describe the vibro-acoustic responses of the system were established by using space-harmonic series expansions and the principle of virtual work. The periodic model was shown to reduce to the smeared model if the reflected flexural waves at each stud connection are ignored. Convergence of the solution was checked, and the minimum number of terms needed in the series expansion for the solution to converge was obtained as a function of frequency. The predictions were compared with existing test data for steel plates with wooden stiffeners, and reasonable agreement was obtained.

By studying representative numerical results from the two models, the various physical mechanisms influencing STL were explored. The smeared model predicts relatively simple behaviour, in which the only conspicuous features were associated with coincidence effects with the two types of structural wave allowed by partition model, and internal resonances of the air between the panels. In the periodic model, many more features were evident, associated with the structure of pass- and stop-bands for structural waves in the partition.

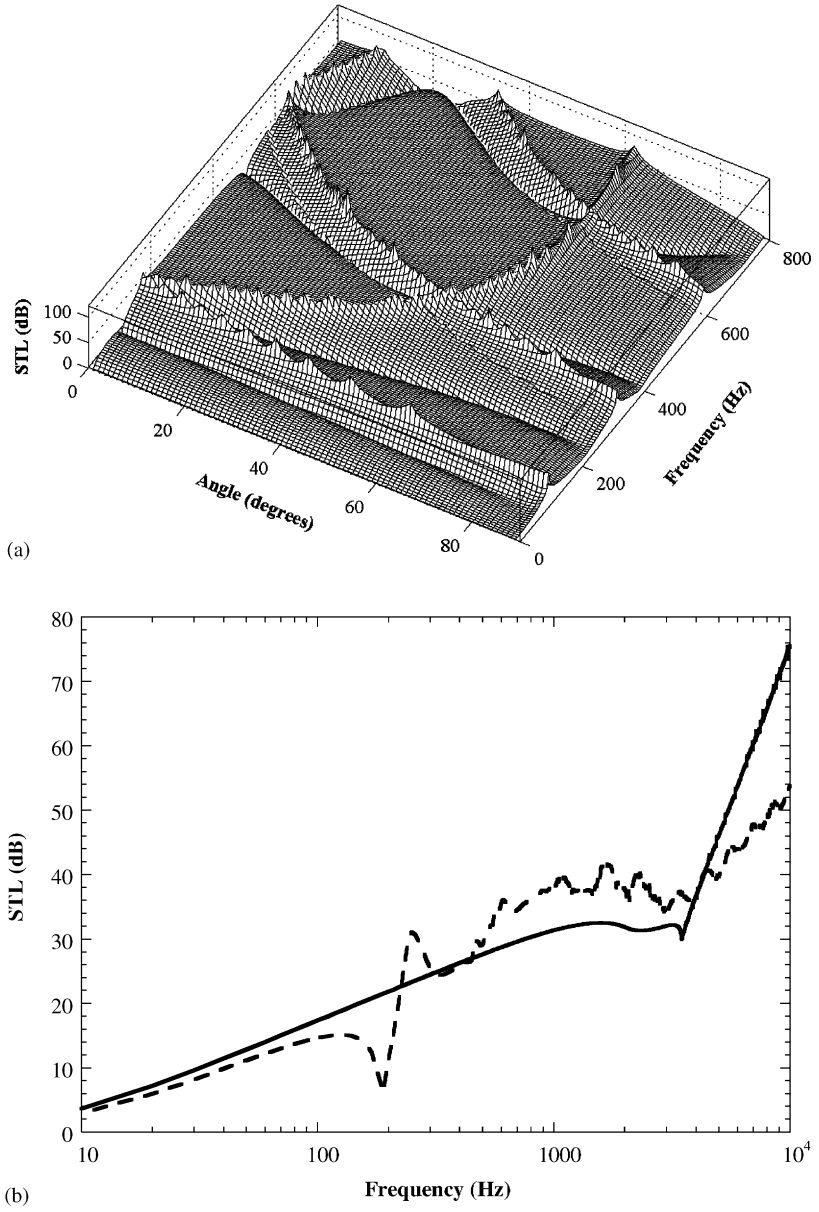

Fig. 13. (a) The variation of the STL with incidence angle for the periodic model. (b) The average of the STL over incidence angle for both the periodic and smeared models. Solid line: smeared model; dashed line: periodic model.

The main aim of the present investigation has been to establish analytical modelling for the study of sound transmission across double-leaf partitions, and to understand the underlying physics of the results obtained. The models presented here have made many simplifications. The sound field was assumed to be restricted to the horizontal plane only, and many complicating

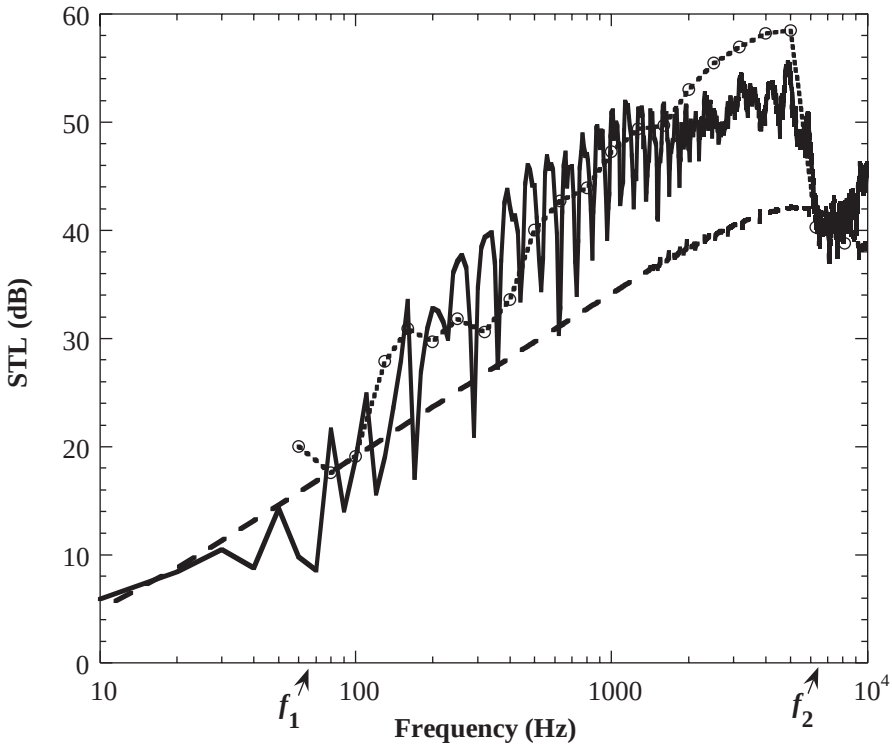

Fig. 14. Comparison of STL predictions from both the smeared model and the periodic model with test data taken from Fig. 12 of Hongisto et al. [24]. Solid line: periodic model; dashed line: smeared model; small circles: experimental measurements.

Table 2
Simulation data for steel plates with wooden studs

K_t (N/m)	2.99×10^{10}	K_r (Nm/rad)	1.5×10^6	M (kg)	1.942
L (m)	1.100	E_1 (Pa)	2×10^{11}	E_2 (Pa)	2×10^{11}
ρ_0 (kg/m^3)	1.21	ρ_1 (kg/m^3)	7800	ρ_2 (kg/m^3)	7800
h_2 (m)	2×10^{-3}	h_1 (m)	2×10^{-3}	η_1	0.0006
η_2	0.0006	ν_1	0.28	ν_2	0.28
c_0 (m/s)	343				

features of real partitions were disregarded: finite size of wall, connection details around the edges, joins between board panels, discrete screw fixings of panels to studs, exact periodicity of stud spacings, and so on.

It is intended that these important details will be considered in future work which will extend this study and open the way to optimisation of partition design for most effective soundproofing. Some of the features are relatively easy to incorporate, but others will require significant changes. In particular, relaxing the assumption of periodicity is difficult. Given the current state of theories of vibration of such structures, it would force the model either to become purely numerical, or else

to become statistical in nature: see, e.g., Refs. [26,27]. Nevertheless, the qualitative effects expected from non-periodicity are understood, so-called "Anderson localisation", and it will be an interesting target for future research to quantify whether such effects are important for realistic building structures.

Acknowledgements

The authors thank the UK Engineering and Physical Sciences Research Council and Banro Holdings Ltd. for financial support of this project.

References

[1] L. Beranek, G.A. Work, Sound transmission through multiple structures containing flexible blankets, *Journal of the Acoustical Society of America* 21 (4) (1949) 419–428.
[2] A. London, Transmission of reverberant sound through double walls, *Journal of the Acoustical Society of America* 22 (2) (1950) 270–279.
[3] K.A. Mulholland, H.D. Parbrook, A. Cummings, The transmission loss of double panels, *Journal of Sound and Vibration* 6 (3) (1967) 324–334.
[4] F. Fahy, *Sound and Structural Vibration Radiation, Transmission and Response*, Academic Press, London, 1987.
[5] W. Kropp, E. Rebillard, On the air-borne sound insulation of double wall constructions, *Acta Acustica* 85 (1999) 707–720.
[6] L. Brillouin, *Wave Propagation in Periodic Structures*, Dover, New York, 1953.
[7] D.J. Mead, Wave propagation in continuous periodic structures: research contributions from Southampton, 1964–1995, *Journal of Sound and Vibration* 190 (3) (1996) 495–524.
[8] G.P. Mathur, Bio.N. Tran, J.S. Bolton, N.-M. Shiau, Sound transmission through stiffened double-panel structures lined with elastic porous materials, *Proceedings of the 14th DGLR/AIAA Aero-Acoustics Conference*, 1992, pp. 102–105.
[9] B.H. Sharp, Prediction methods for the sound transmission of building elements, *Noise Control Engineering* 11 (1978).
[10] L. Cremer, M. Hechl, *Structure-Borne Sound: Structural Vibrations and Sound Radiation at Audio Frequencies* (translated and revised by E.E. Ungar), Springer, Berlin, 1973.
[11] W. Desmet, P. Sas, Sound transmission of finite double-panel partitions with sound absorbing material and panel stiffeners, *Proceedings of the First Joint CEAS/AIAA Aero-Acoustical Conference (16th AIAA Aero-Acoustical Conference)*, AIAA-95-043, 1995.
[12] E.H. Dowell, G.F. Gorman III, D.A. Smith, Acoustoelasticity: general theory, acoustic natural mode and forced response to sinusoidal excitation, including comparisons with experiment, *Journal of Sound and Vibration* 52 (4) (1977) 519–542.
[13] G.-F. Lin, J.M. Garrelick, Sound transmission through periodically framed parallel plates, *Journal of the Acoustical Society of America* 61 (1977) 1014–1018.
[14] V.N. Evseev, Sound radiation from an infinite plate with periodic inhomogeneities, *Soviet Physics Acoustics* 19 (1973) 345–351.
[15] I.A. Urusovskii, Sound transmission through two periodically framed parallel plates, *Journal of Soviet Physics Acoustics* 38 (4) (1992) 411–413.
[16] D.J. Mead, Free wave propagation in periodically supported, infinite beams, *Journal of Sound and Vibration* 11 (2) (1970) 181–197.
[17] D.J. Mead, K.K. Pujara, Space-harmonic analysis of periodically supported beams: response to convected random loading, *Journal of Sound and Vibration* 14 (4) (1971) 525–541.

[18] D. Takahashi, Sound radiation from periodically connected harmonic double-plate structures, *Journal of Sound and Vibration* 90 (4) (1983) 541–557.
[19] D.J. Mead, Vibration response and wave propagation in periodic structures, *Journal of Engineering for Industry* 93 (series B) (1971) 783–792.
[20] J.-H. Lee, J. Kim, Analysis of sound transmission through periodically stiffened panels by space harmonic expansion method, *Journal of Sound and Vibration* 251 (2) (2002) 349–366.
[21] A.C. Nilsson, Some acoustical properties of floating floor constructions, *Journal of the Acoustical Society of America* 61 (1977) 1533–1539.
[22] *CES Selector* Version 4.0, Granta Design Limited, Cambridge, UK.
[23] M.P. Norton, *Fundamentals of Noise and Vibration Analysis for Engineers*, Cambridge University Press, Cambridge, 1989.
[24] V. Hongisto, M. Lindgren, R. Helenius, Sound insulation of walls—an experimental parametric study, *Acta Acustica* 88 (2002) 904–923.
[25] D.J. Allwright, M. Blakemore, P.R. Brazier-Smith, J. Woodhouse, Vibration transmission through symmetric resonant couplings, *Philosophical Transactions of the Royal Society of London A* 346 (1994) 511–524.
[26] C.H. Hodges, J. Woodhouse, Vibration isolation from irregularity in a nearly-periodic structure: theory and measurements, *Journal of the Acoustical Society of America* 74 (1983) 894–905.
[27] C.H. Hodges, J. Woodhouse, Theories of noise and vibration transmission in complex structures, *Reports on Progress in Physics* 49 (1986) 107–170.